ACS OMEGA

Open Access

http://pubs.acs.org/journal/acsodf

Article

Tyrosine Mutation in the Characteristic Motif of the Amorphous Region of Spidroin for Self-Assembly Capability Enhancement

Ziyang Chen, Cheng Cheng,* Li Liu, Baoyang Lin, Yongji Xiong, Weiyu Zhu, Ke Zheng,* and Bingfang He

Cite This: *ACS Omega* 2024, 9, 22441−22449

Read Online

ACCESS | Metrics & More | Article Recommendations | Supporting Information

ABSTRACT: Spidroin, with robust mechanical performance and good biocompatibility, could fulfill broad applications in material science and biomedical fields. Development of miniature spidroin has made abundant fiber production economically feasible, but the mechanical properties of artificial silk still fall short of natural silk. The mechanism behind mechanical properties of spidroin usually focuses on β-microcrystalline regions; the effect of amorphous regions was barely studied. In this study, residue tyrosines (Y) were designed to replace asparagine (N)/glutamic acid (Q) in the characteristic motifs (GGX)n in amorphous regions for performance enhancement of spidroin; the mutants presented lower free energy and significantly exhibited stronger van der Waals and electrostatic interactions, which might result from $\pi-\pi$ stacking interactions between the phenyl rings in the side chain of tyrosine. Additionally, the soluble expressions of wild-type spidroin and mutant spidroin were achieved when heterologously expressed in *E. coli*, with yields of 560 mg/L (2REP), 590 mg/L (2REPM), 240 mg/L (4REP), and 280 mg/L (4REPM). Significantly, secondary structure analysis confirmed that the mutant spidroin more avidly forms more β-sheets than the wild-type spidroin, and aggregation morphology suggested that mutant spidroin displayed better self-assembly capacity and was easier to form artificial spider silk fibers; in particular, self-assembled 4REPM nanofibrils had an average modulus of 11.2 ± 0.35 GPa, about 2 times higher than self-assembled *B. mori* silk nanofibrils and almost the same as that of native spider dragline silk fibers (10−15 GPa). Thus, we first demonstrated a new influence mechanism of the amorphous region's characteristic motif on the self-assembly and material properties of spidroin. Our study provides a reference for the design of high-performance material proteins and their heterologous preparation.

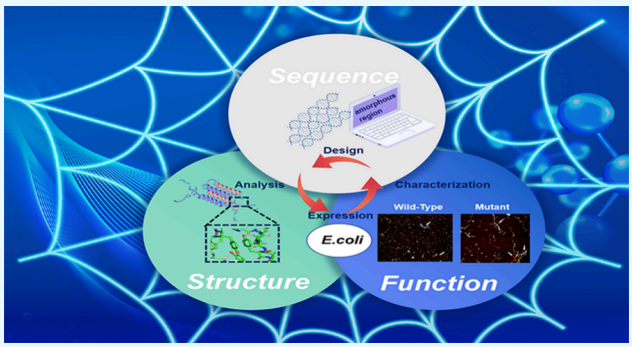

1. INTRODUCTION

Spider silk, especially major ampullate silk, possesses the highest tensile strength and toughness among animal fibers, earning it the reputation of "biological steel". Its excellent mechanical properties and biocompatibility have attracted significant attention. Research and applications of spidroin-based materials have gradually expanded into high-tech fields. We developed a novel, highly elastic, intelligent programmable woven textile (i-SPT) with wound management and motion monitoring functions based on spidroin.[1] Spidroin can also be used as nerve conduits, substitutes for blood vessels, and even in the preparation of photoresists for achieving ultrahigh-precision 3D electron beam lithography.[2−4]

Spider silk is composed of spidroin that undergoes hierarchical assembly, resulting in ordered structural features from the nanoscale to the macroscale. Natural spidroins possess shared or similar primary structural patterns, composed of three structural domains, including highly conserved N/C-terminal nonrepetitive domains (NT/CT) and a central repetitive core domain (REP).[5−8] The primary structure (amino acid sequence) of spidroin serves as the foundation of fiber assembly, closely related to its structure and properties. The REP domain constitutes approximately 90% of the amino acid composition of spidroins, serving as the predominant portion of their sequences. The characteristics of spidroins, such as their ultrahigh molecular weight, excessively high content of specific amino acids, and highly repetitive sequence motifs within the REP, contribute to the challenges in heterologous expression using artificial synthesis systems. Issues such as premature termination, low yields, and expression instability often hinder their production.[9,10] Furthermore, the high GC content and suboptimal codon usage in natural spidroin sequences further limit their

Received: March 13, 2024
Revised: April 12, 2024
Accepted: April 26, 2024
Published: May 10, 2024

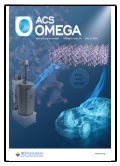

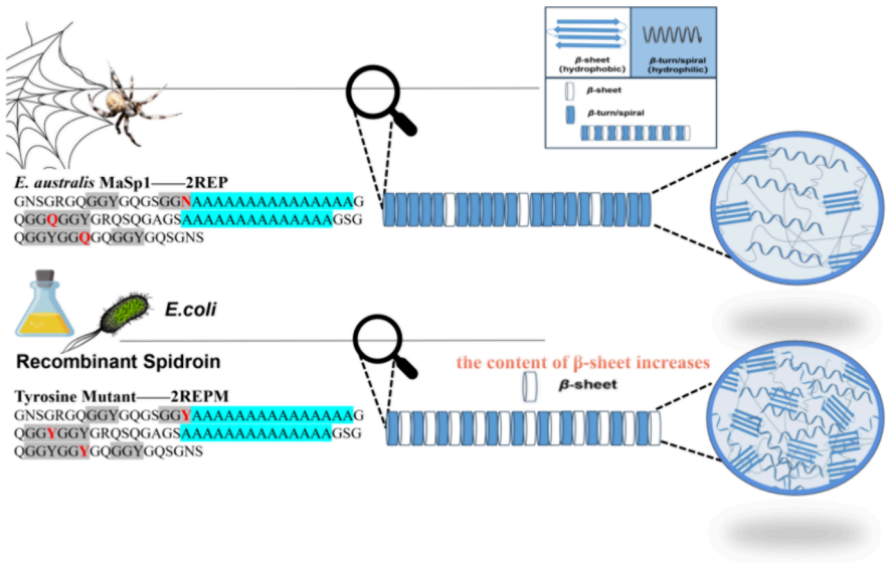

Figure 1. Schematic diagram of wild-type spidroin (2REP) and mutant spidroin (2REPM) and the molecular structures of these self-assembled spidroins

compatibility with synthetic systems. Advancements in genetic engineering and synthetic biology have made it feasible to synthesize custom-designed artificial spider silk materials.[9−11] Recombinant spidroins (284.9 kDa) were synthesized by metabolic engineering. Chimeric spidroin based on highly soluble and pH-responsive terminal domains and repetitive unit domains was constructed in our previous study; efficient biosynthesis of spidroin was achieved in *E. coli*.[1] However, the mechanical performance of recombinant spidroins has yet to attain substantial improvement.[9]

The repetitive units of spidroin serve as the fundamental modules for creating multiscale assemblies. These units consist of alternating regions of crystalline and semiamorphous regions. Spidroins are naturally designed as block copolymers with alternating hydrophilic and hydrophobic segments.[5−8] The repetitive unit motifs play a crucial role in the outstanding mechanical properties of spider silk.[12,13] The characteristic motifs, such as A_n or $(GA)_n$, are responsible for the reverse parallel β-sheet structures within the microcrystalline regions of spider silk, contributing to its high strength.[14,15] The motifs $(GGX)_n$, on the other hand, mainly form 3_{10}-helices in the semiamorphous regions, promoting the high extensibility and high Young's modulus of spider silk.[16−18]

It is worth noting that existing studies have mainly focused on the length of the repetitive unit and the structural characteristics of the microcrystalline region of spidroins. The impact of the amorphous region on self-assembly and mechanical properties has received limited attention. Li et al. leveraged the propensity of three different types of amyloid-like proteins to form β-sheet structures. The characteristic motifs of spidroin in the β-crystalline region were substituted with those of amyloid-like proteins. The resulting recombinant proteins, incorporating the amyloid-like protein motifs (FGAILSS), achieved a remarkable tensile strength of 0.98 GPa and an average toughness of 161 MJ/m^3 in biomimetic spider silk fibers, surpassing the majority of recombinant protein fibers and even some natural spider silk fibers.[19] Rising et al. aimed to enhance the propensity of the repetitive unit motif (A_n) to form β-sheet structures. They selectively introduced genetic mutations involving Ile and Val. The resultant recombinant proteins, with the artificial, repetitive unit motif $(A_3I)_3$-A_{14}, exhibited significantly improved mechanical properties in biomimetic spider silk.[12,20,21] Despite some progress in the modification and design of spidroin, artificial spider silk still falls short in terms of mechanical performance compared with natural spider silk. This might be attributed to the imperfect β-sheet structure formed by the characteristic motif A_n of the recombinant spidroin, which transformed into an α-helical structure during the spinning process.[22−24] Currently, design theories and methods to improve the performance of spidroins through sequence design are notably lacking.

This study is based on the repetitive units (2REP) derived from *E. australis* MaSp1 as the framework, aiming to enhance the performance of the spidroins. The amorphous regions of the repetitive units were designed and modified to increase the content of tyrosine Y (N154Y, Q174Y, and Q212Y) in the characteristic motif $(GGX)_n$. The schematic diagram of the wild-type and mutant spidroin and the molecular structure of these self-assembled recombinant spidroins are presented in Figure 1. Evaluated by molecular dynamics simulations, the van der Waals and electrostatic interactions were stronger after increasing more tyrosine in the sequence, especially $\pi-\pi$ stacking interaction. Further, a tetramer spidroin and its mutants were constructed and expressed in *E. coli* to demonstrate better the effect of the increasing numbers of Y mutants. The self-assembly ability and morphology of the obtained spidroin were characterized after Ni sepharose purification, and the results revealed that the modification of the repetitive amorphous regions significantly contributed to the enhancement of the self-assembly capability of spidroin, facilitating the formation of fiber aggregates. This ultimately leads to an improvement of the mechanical properties of spider silk materials. This research provides guidance for the design of high-performance biomimetic spidroin and lays the foundation for the development of premium material proteins.

2. RESULTS AND DISCUSSION

2.1. Mutant Artificial Spidroin Designed by Molecular Dynamic Analysis. Based on 3D structure prediction using Rosetta Design,[12] we analyzed the Rosetta potential energy of

https://doi.org/10.1021/acsomega.4c02477
ACS Omega 2024, 9, 22441−22449

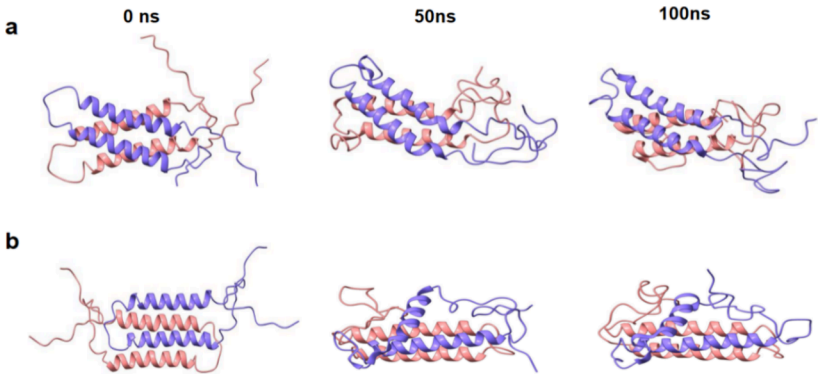

Figure 2. Snapshots of 2REP (a) and 2REPM (b) dimers at 0, 50, and 100 ns.

the microcrystalline and amorphous regions of the spidroin before and after the mutation. It was observed that after increasing the content of tyrosine in the amorphous region by substituting asparagine/glutamic acid with tyrosine (N154Y, Q174Y, and Q212Y) in the microcrystalline region, this mutant effectively reduced the Rosetta potential energy (ΔG) from −24.6 to −25.6 kcal/mol, which shows the increasing likelihood of fiber formation (Figure S1). Subsequently, dimeric forms of 2REP and 2REPM (N154Y, Q174Y, and Q212Y) were constructed using HDOCK. The best binding modes of 2REP and 2REPM dimers are with scores of −195.22 and −230.91, respectively, which suggested that the dimeric forms of 2REPM exhibited stronger affinity (Figure 2). During the molecular dynamic simulation, the snapshots of 2REP and 2REPM mutant dimers at 0, 50, and 100 ns are presented in Figure 2. The root-mean-square deviation (RMSD) and the radius of gyration (R_g) of the 2REP/2REPM dimers presented fluctuations within an acceptable range, suggesting that both dimers tend to stabilize during the simulation progresses (Figure S2).

The change in the binding free energy between the 2REP/2REPM dimers over time is shown in Figure 3a. The data from the last 10 ns were analyzed, and the average binding free energy for the 2REP dimer was determined to be −113.11 kcal/mol, while the average binding free energy for the 2REPM dimer was −145.09 kcal/mol. This suggested a stronger affinity between the 2REPM spidroin molecules comparing with the wild-type 2REP spidroin molecules. Of note, the van der Waals, electrostatic, polar solvation, and nonpolar solvation energy contributions to the binding free energy for 2REP dimers were −171.95, −72.90, 146.95, and −15.21 kcal/mol, respectively, while the 2REPM dimers exhibited stronger van der Waals and electrostatic interactions than the 2REP dimer, with van der Waals, electrostatic, polar solvation, and nonpolar solvation energy contributions of −211.85, −93.66, 178.75, and −18.33 kcal/mol, respectively.

Subsequently, the number of hydrogen bonds between the 2REP/2REPM dimers and the number of hydrogen bonds between 2REP/2REPM dimers and the water solvent were calculated (Figure 3b). The data from the last 10 ns were analyzed; the average number of hydrogen bonds for the 2REP/2REPM dimer was determined to be 12.8 and 9.4, respectively, and the average number of hydrogen bonds between the 2REP/2REPM dimer and the water solvent was found to be 271.4 and 240.6, respectively. The decrease in the number of hydrogen bonds indicated a relative weakening of hydrogen-bonding forces. When the number of hydrogen bonds decreases, the contribution of van der Waals interactions becomes more significant. This is consistent with the change in binding free energy between the 2REP/2REPM dimer mentioned in the previous text. The decrease in the number of hydrogen bonds can lead to a more significant contribution of van der Waals interactions in dimer binding, resulting in changes in the binding free energy. As for the increase of van der Waals force, the two engineered spidroins (2REP and 2REPM) differed by three Tyr residues (N154Y, Q174Y, and Q212Y) (Figure 1); the side-chain aromatic rings of Tyr residues of the A chain and B chain of the mutant spidroin dimer (2REPM) are speculated to lead to stronger $\pi-\pi$ stacking interaction than native spidroin dimer (2REP) (Figure 3c). Therefore, the mutant chimeric spidroin is expected to enhance the aggregation capabilities of the spidroin and the likelihood of silk formation.

2.2. Expression and Purification of Spidroin Chimeric Dimers, Tetramers, and Their Mutants (2REPM, 4REPM).

The expression conditions of the four kinds of chimeric spidroin recombinant strains were optimized under the conditions of 0.3 mM IPTG inducing at 25 °C for 24 h. The soluble components of four kinds of chimeric spidroin accounted for 26% (2REP), 33% (2REPM), 13% (4REP), and 16% (4REPM) (Figures 4a and 4b). The solubility of mutant 2REPM/4REPM was higher than that of wild-type 2REP/4REP when it was heterologously expressed in *E. coli*. As shown in Figures 4c and 4d, the purity of four kinds of chimeric spidroins reached above 95% by gray scanning. The concentrations of four types of chimeric spidroin after purification were 560 mg/L (2REP), 590 mg/L (2REPM), 240 mg/L (4REP), and 280 mg/L (4REPM). The yield of spidroin chimeric dimers was higher than tetramers, which might have resulted from the increased metabolic pressure caused by the length of the spidroin sequence, which is also observed in published heterologous expression of spidroin.[32] It is generally believed that the molecular weight of spidroin is negatively correlated to the heterologous expression.[33] Subsequently, the four types of chimeric spidroins were concentrated to 100 mg/L at room temperature for further characterization.

2.3. Increasing Self-Assembly Capability and β-Sheet Conformation of Mutant Spidroin (2REPM and 4REPM).

The repetitive domains in the recombinant spidroin sequence are believed to contribute to the formation of β-sheets as well as the nanofibril formation; the interaction and morphology of the assembly of these recombinant spidroins need further evaluated.[34−38] Therefore, we further investigated the self-

https://doi.org/10.1021/acsomega.4c02477
ACS Omega 2024, 9, 22441−22449

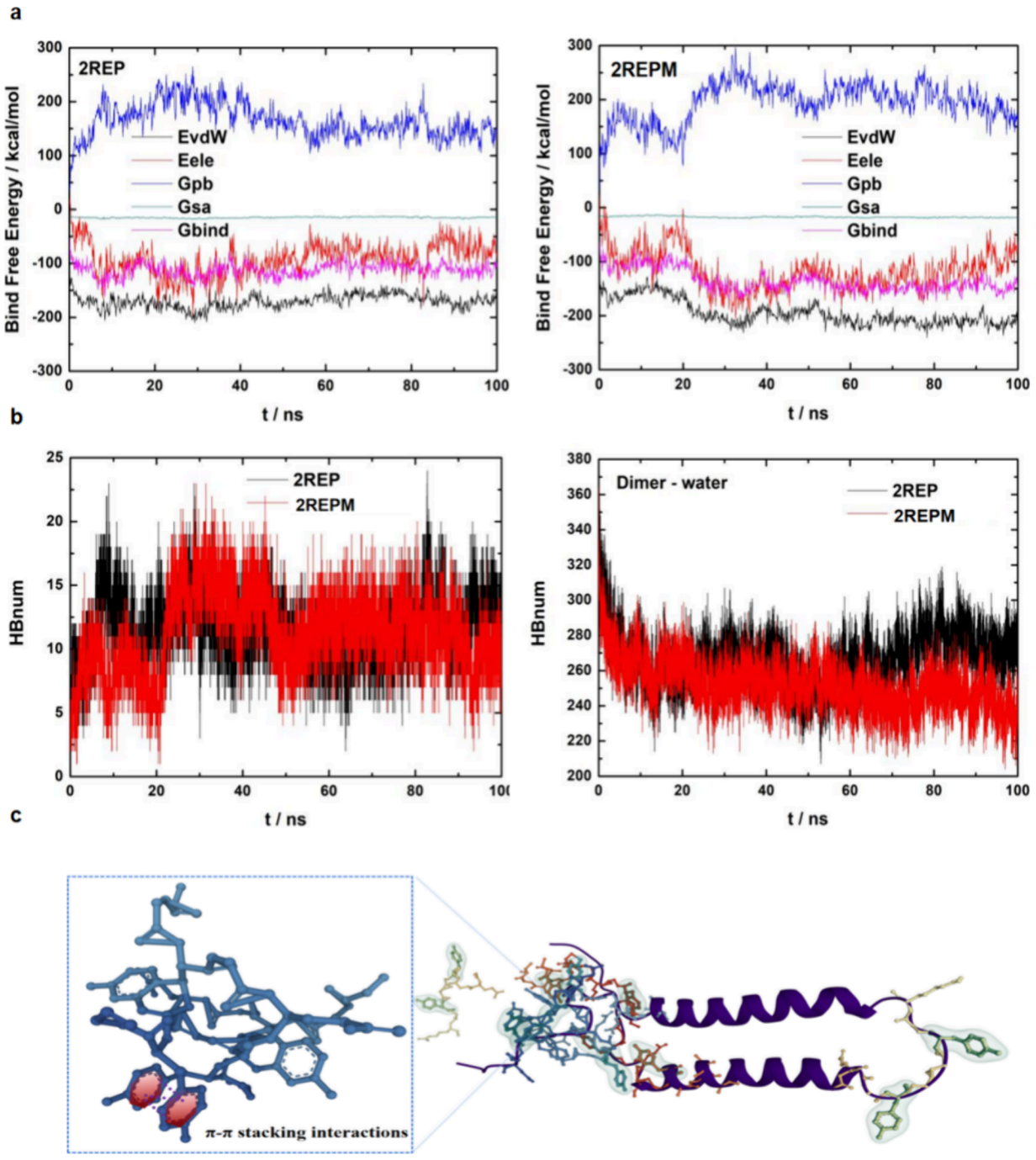

Figure 3. (a) Binding free energy of the 2REP dimer and 2REPM dimer. (b) Number of hydrogen bonds between the 2REP/2REPM dimer and between the 2REP/2REPM dimer and the water solvent. (c) Possible $\pi-\pi$ stacking interaction of the Tyr residues with a side-chain aromatic ring.

assembly of these recombinant spidroins by AFM observation. The morphologies of the resultant self-assemblies are shown in Figure 5. In general, the self-assembly of four kinds of chimeric spidroin followed a heterogeneous nucleation progress where spidroin molecules first folded into nanoparticles and then these nanoparticles assembled into nanofibrils. The preliminary nanoparticles appeared in the early stages of protein self-assembly. However, the self-assembled 2REP spidroins presented well-dispersed nanoparticles with a diameter of 4−6 nm after incubating the spidroins at 60 °C for as long as 96 h (Figure 5a). The results demonstrated that those 2REP spidroins were hard to self-assemble into nanofibrils under our conditions. This is reasonable because the relatively small size of the repetitive domains in 2REP spidroins (∼7.07 kDa) was unfavorable in initializing their fibrillar formation, although the formation of nanoparticles accompanied by network fibrils was indicated in the self-assembled 4REP spidroins. As shown in Figure 5c, the diameter of these network fibrillar structures was approximately 1.0 nm, which was only at the level of molecular chains. The appearance of these fibrillar structures suggested that the 4REP spidroins with a higher molecular weight of 14.3 kDa still barely self-assembled into nanofibrils. Interestingly, the molecular weight of 2REPM spidroins was comparable to that of the 2REP spidroins. However, the 2REPM spidroins were capable of self-assembling into short nanofibrils with a diameter of 8−10 nm (Figure 5b).

https://doi.org/10.1021/acsomega.4c02477
ACS Omega 2024, 9, 22441−22449

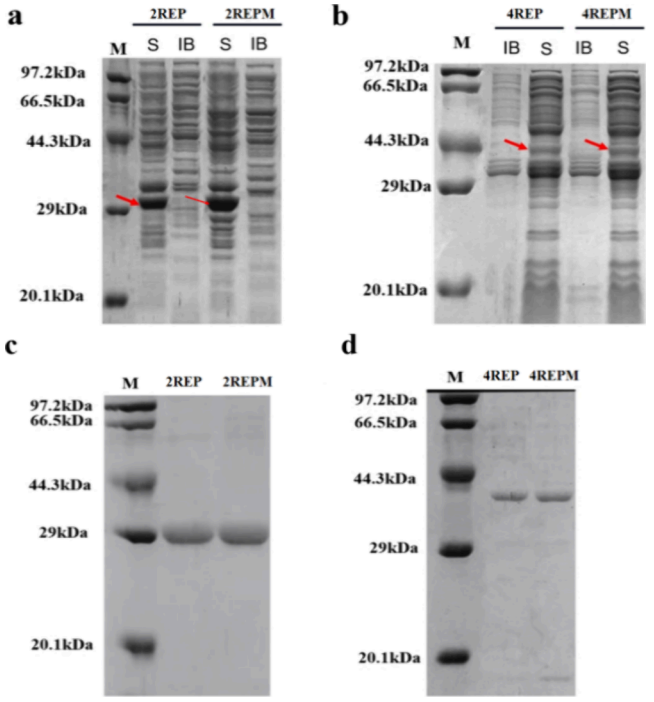

Figure 4. Expression and purification of four types of chimeric spidroins. (a) Expression of 2REP and 2REPM (MW: 33.2 kDa). (b) Expression of 4REP and 4REPM (MW: 40.1 kDa). (c) Purification of 2REP and 2REPM (MW: 33.2 kDa). (d) Purification of 4REP and 4REPM (MW: 40.1 kDa). Key: protein marker (M); S stands for soluble fractions; IB stands for inclusion bodies.

Consequently, an expected formation of nanofibrils several microns in length (Figure 5d) was presented in the self-assembled 4REPM spidroins. It is worth mentioning that the self-assembled 4REPM nanofibrils had an average modulus of 11.2 ± 0.35 GPa, about 2 times higher than self-assembled *B. mori* silk nanofibrils[32] and almost the same as the modulus of native dragline silk fibers (10−15 GPa).[33]

The remarkable mechanical performance of these nanofibrils suggesting the advantages of portion folding were aggregated in the 4REPM spidroins. Thereafter, circular dichroism (CD) spectroscopy was employed to characterize the molecular structures of these self-assembled recombinant spidroins. As shown in Figures 6a and 6b, the CD spectra of 2REP and 4REP were similar, where strong negative peaks appearing at around 207 and 223 nm, as well as a positive peak appearing at around 193 nm, indicated that the molecular conformations of the two spidroins were mainly α-helix and random coil structures. For comparison, a clear shift of the positive peak to 199 nm and a broad negative peak around 220 nm were presented in the mutated spidroins 2REPM and 4REPM, indicative of the β-sheet conformation. Moreover, the negative peak at 223 nm suggested a partial remaining of the α-helix conformation in these mutant spidroins. The HT curves in the Supporting Information were presented to clarify the reproducibility of CD signals (Figure S3). In Figure 6, a deconvolution of the FTIR spectra (amide I band) was performed to analyze the secondary structures of the 2REP and 2REPM spidroins. The absorption peaks at 1685, 1655, and 1628 cm^{-1} are assigned to the β-turn, random coil/helix, and β-sheet conformation, respectively. As expected, a higher β-sheet content of 32.3% was presented in 4REPM (Figure 6f), whereas a higher β-sheet content of 25.4% was presented in 4REP (Figure 6e). The same tendency of the spidroin conformation was also indicated in 2REP and 2REPM, where 15.6% (Figure 6c) and 27.2% (Figure 6d) β-sheet content was presented, respectively. In particular, both the CD and FTIR spectra showed a good agreement with the results in the AFM observation, where the mutated spidroins were significantly self-assembled into nanofibrils. Modifying the characteristic motif in the amorphous region, which adjacent sequences in the microcrystalline region, significantly increases the formation of β-sheet content and contributes to the self-assembly capability of spidroin. Therefore, comparing the β-sheet conformation and the self-assembly capability between the wild-type spidroin and mutant spidroin serves as a good

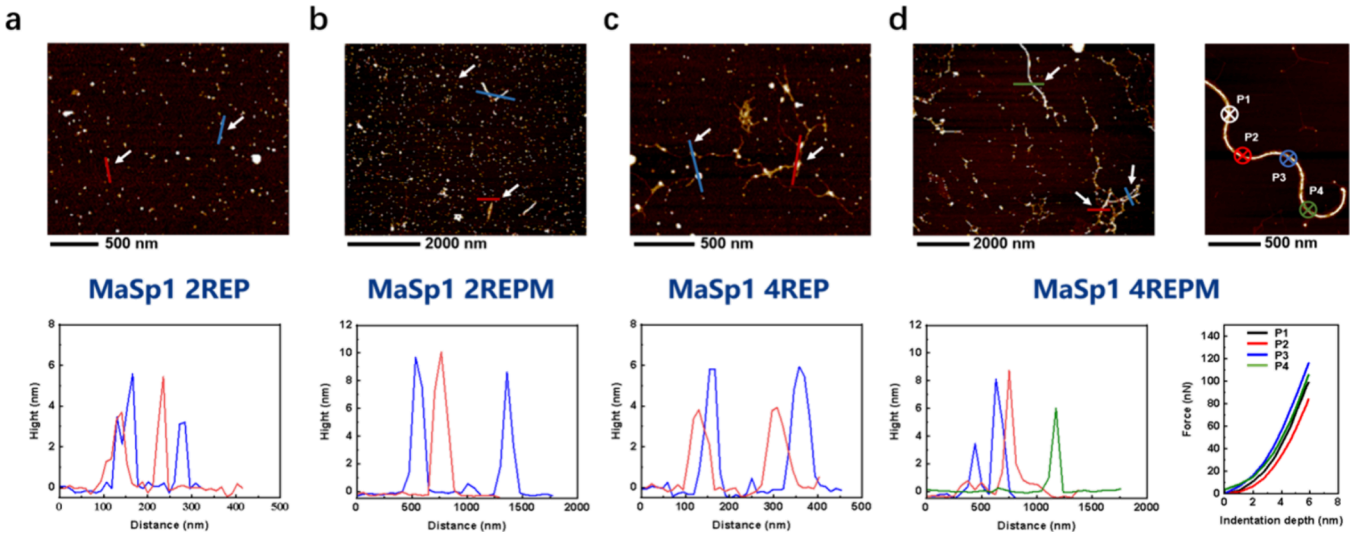

Figure 5. Morphologies and size distributions of the resultant self-assemblies of (a) 2REP and (b) 2REPM spidroins. (c) Morphology and size distribution of the resultant self-assemblies of 4REP spidroins. (d) Morphology and mechanical properties of the resultant self-assemblies of 4REPM spidroins.

https://doi.org/10.1021/acsomega.4c02477
ACS Omega 2024, 9, 22441−22449

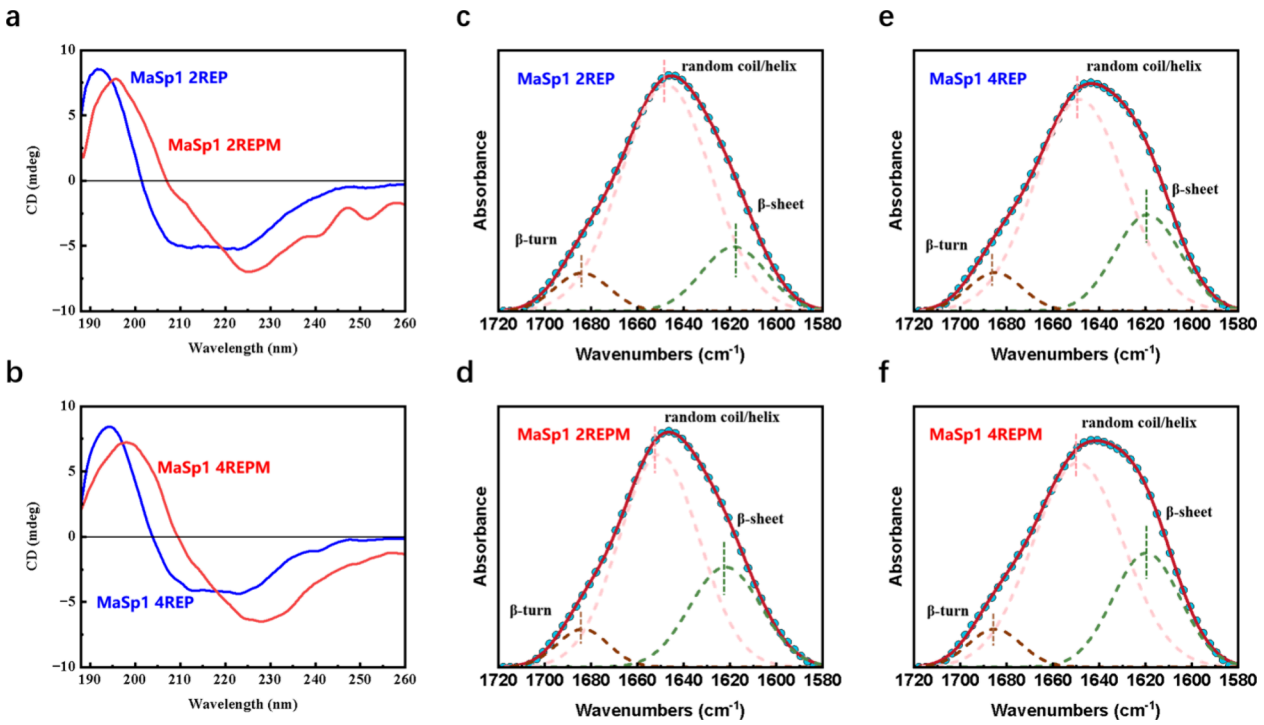

Figure 6. CD spectra of (a) 2REP/2REPM and (b) 4REP/4REPM spidroins. Deconvolution results of the amide I band of self-assembled (c) 2REP, (d) 2REPM, (e) 4REP, and (f) 4REPM spidroins.

verification of the Rosetta Design and molecular dynamic analysis in Figure S1 and Figure 3.

3. CONCLUSION

Spiders are carnivorous arthropods and cannot be raised for silk production like silkworms; heterologous biosynthesis becomes the only way to obtain large quantities of spider silk. However, the high molecular weight, high sequence repetition, and specific amino acid content of natural spidroins lead to low production yields and unstable expressions, posing significant challenges in the biosynthesis of spider silk materials. Furthermore, the unclear correlation between the characteristic motif-structure assembly and mechanical properties of spidroins hinders the effective functional enhancement. Existing studies have mainly focused on the length of the repetitive unit and the replacement of characteristic motifs in the microcrystalline region of spidroins to enhance the mechanical performance while neglecting the influence of the amorphous region which adjacent sequences in the microcrystalline region on their self-assembly and mechanical properties. This does not meet the requirements for the design and modification of biomimetic spidroins.

Interestingly, this study focused on the design and engineering of the repetitive unit amorphous region sequence $(GGX)_n$ of a low molecular weight recombinant spidroin (2REP), which served as the backbone. Mutations (N154Y, Q174Y, and Q212Y) were introduced to increase the tyrosine content of the characteristic region in the amorphous region of the repetitive units of spidroin. Molecular dynamics simulations confirmed a significant increase in the binding free energy after the mutations. Additionally, a spidroin dimer mutant (2REPM), tetramer, and its mutant (4REP, 4REPM) were constructed through genetic mutations to examine the effect of the repeat number on the mechanical properties of spidroin. The tyrosine of the characteristic motif $(GGX)_n$ in the amorphous region effectively enhanced the $\pi-\pi$ stacking interactions within the molecule, strengthening the proximity to the neighboring β-sheet crystalline region. The soluble expressions of wild-type spidroin and mutant spidroin were achieved when heterologously expressed in *E. coli*, with yields of 560 mg/L (2REP), 590 mg/L (2REPM), 240 mg/L (4REP), and 280 mg/L (4REPM). Subsequently, the morphologies and size distributions of the resultant self-assemblies of 2REP and 2REPM spidroins and 4REP and 4REPM spidroins were analyzed. The appearance of these fibrillar structures suggested that the 2REP/4REP spidroins barely self-assembled into nanofibrils. However, the mutant 2REPM spidroins, with a comparable molecular weight to that of 2REP spidroins, were capable of self-assembling into short nanofibrils with a diameter of 8−10 nm. Significantly, the mutant 4REPM spidroins self-assembled into nanofibrils with several microns in length, and the self-assembled 4REPM nanofibrils showed an average modulus of 11.2 ± 0.35 GPa, about 2 times higher than self-assembled *B. mori* silk nanofibrils and almost the same as the modulus of native dragline silk fibers (10−15 GPa). These characterization experiments demonstrated a significant increase in β-sheet content and enhanced the self-assembly ability of the engineered mutant recombinant spidroin.

The β-sheet microcrystalline structure formed by the self-assembly of repetitive units is crucial for the mechanical properties of spider silk. Based on molecular dynamics simulations and comprehensive analysis of the impact of the amorphous region sequence on the stability of the microcrystalline structure, this study found that the amorphous region significantly contributes to the formation and stability of the microcrystalline structure and its self-assembly and mechanical properties, which elucidate its correlation with self-assembly and performance. Our study provides molecular theoretical guidance for designing high-performance and easily

https://doi.org/10.1021/acsomega.4c02477
ACS Omega 2024, 9, 22441−22449

expressed biomimetic spidroin repetitive unit characteristic motifs. Though numerous efforts have been devoted to the recombinant production of spidroin in prokaryotic cells, issues such as the high molecular weight and large repetitive DNA sequences of spidroin still hinder its highly efficient expression. This study provides a reference strategy for the soluble expression of spidroin and its mutants. While promising, future research is warranted to further improve the yield by some techniques, such as metabolic engineering of the host and codon optimization. Another direction worth taking is the exploration of the biomedical application of spidroin, especially the mutant spidroin with better self-assembly capacity. In addition, we believe that the development of rational design methods for high-performance artificial spidroin would not only contribute to fundamental research in the field of spider silk materials but also support the future development and manufacturing of next-generation materials, such as biomembranes, artificial skin, and biodegradable scaffolds, based on spidroin as a building block material.

4. MATERIALS AND METHODS

4.1. Molecular Dynamics Simulation. Molecular dynamics (MD) simulations of the 2REP and 2REPM dimer system were performed using the GROMACS 2021.5 package.[25] The spidroin 2REP and mutant 2REPM were parametrized by the Amberff14sb force field.[26] The likely binding models of the dimer were explored by HDOCK,[27] and the top 1 docking model was used for further MD simulation; the results were visualized by UCSF ChimeraX.[28]

A cubic box was established by extending at least 1.4 nm outward along 2REP/2REPM dimer ($12 \times 12 \times 12$ nm^3); then the system was solvated in TIP3P water, and 4 Cl^- was added to keep the solution electrically neutral. Energy minimization was performed by using the steepest descent algorithm with a force tolerance of 500 kJ mol^{-1} nm^{-1}. In all three directions, periodic boundary conditions were imposed. The system was relaxed for 1 ns under NPT ensemble, and positional restraints with a constant of 1000 kJ mol^{-1} nm^{-2} in three directions were performed on heavy protein atoms. After the above steps were completed, a 100 ns NPT MD simulation was performed. The pressure was maintained at 1 bar by the Parrinello−Rahman barostat[29] in an isotropic manner, and temperature was maintained at 333 K by the V-rescal thermostat.[30] The LINCS algorithm was performed to constrain bond lengths of hydrogen atoms. Lennard-Jones interactions were calculated within a cutoff of 1.2 nm, and electrostatic interactions beyond 1.2 nm were treated with the particle-mesh Ewald (PME) method with a grid spacing of 0.16 nm. Additionally, the binding free energy of inter-2REP/2REPM was analyzed according to the MM/PBSA method by the gmx_MMPBSA tool.[31]

4.2. Construction and Expression of Spidroin Chimera Dimers (2REP), Tetramers (4REP), and Their Mutants (2REPM, 4REPM). The One-Step Cloning Kit and restriction enzymes were purchased from Takara. The plasmid purification, pSE380 plasmid, and gel extraction kits were purchased from Axygen BioScience, Inc. All sequencing was performed by General Biol (Anhui). *E. coli* strain Rosetta (DE3) Chemically Competent Cell was purchased from Invitrogen (USA). The chimeric spidroin gene 2REP consists of NT (gene bank accession number AM259067), CT (gene bank accession number JX513956), and two repeat regions (gene bank accession number AJ973155), which were synthesized by Genewiz (Suzhou, China). All Ni-NTA column protein purification was performed on an ÄKTA pure system.

In this experiment, the chimeric spidroin 2REP (the two terminals of 2REP contain isocaudal enzymes NheI and SpeI) inserted on the cloning vector pUC57 was used as the template, and the single point mutation was used to design appropriate primers for PCR of PUC57-NT-2REP-CT to achieve the purpose of gene site-specific mutation. The X (X = glutamine Q or asparagine N) in chimeric spidroin 2REP at positions 154, 174, and 212 was mutated to Y (tyrosine). The required mutation sequence 2REPM with three mutational sites was obtained by three-primer continuous mutagenesis. The obtained pUC57-NT-2REP-CT and pUC57-NT-2REPM-CT were doubled by the isocaudal enzyme ligation method to obtain tetramers. The plasmid PUC57-NT-2REP-CT was double digested with restriction endonuclease enzymes NheI and SpeI. The tetramer plasmid pUC57-NT-4Rep-CT was obtained by linking the linearized 2REP obtained from DNA recovery with the single enzyme digestion of NheI. The mutational tetramers pUC-NT-4RepM-CT were obtained by the same method. After the screening, four chimeric spidroin genes NT-2REP/2REPM-CT and NT-4REP/4REPM-CT were constructed into 6× His labeled pSE380 expression vectors by one-step cloning. The four constructed plasmids were transformed into *E. coli* strain Rosetta (DE3). The sequencing correct colony was incubated with LB medium (50 mL with 100 μg mL^{-1} ampicillin) in the orbital shaker overnight at 37 °C, then transferred 2% of 50 mL of culture to 100 mL of LB medium with 100 μg mL^{-1} ampicillin, and inoculated at 37 °C until the OD_{600} reached about 0.8. The induction conditions were optimized to 0.3 mM IPTG and 25 °C for 24 h. Finally, the cell pellets were resuspended in Buffer A (20 mM Tris, 300 mM NaCl, pH 8.0) and lysed by sonication followed by centrifugation at 16000*g* at 4 °C for 30 min. The supernatant of cell lysis was loaded into a Ni-NTA column and was sequentially washed by Buffer B (20 mM Tris, 300 mM NaCl, 300 mM imidazole, pH 8.0) with 10%, 20%, and 30% concentration. The Bradford method was used to determine the concentration of chimeric spidroins, with bovine serum albumin used as the standard. For subsequent self-assembly characterization, all four kinds of chimeric spidroins were concentrated. The purified four kinds of chimeric spidroins were centrifuged at 3000 rpm at 4 °C for 15 min using a centrifugal filter unit (Millipore) with a molecular weight of 10 kDa. The operation was repeated until the spidroin solution was ultrafiltered completely to concentrate the spidroins. The concentration of the concentrated chimeric spidroins was determined by the BCA method.

4.3. Atomic Force Microscopy. For atomic force electron microscopy (AFM) measurements, self-assembled recombinant spidroin dispersions were diluted to 0.1 mg/mL by deionized water. 10 μL of the aqueous solution was then added onto a clean mica surface for coating for 120 s, followed by purging with nitrogen gas. The morphologies of the nanoparticles and nanofibrils were observed by an ICON AFM fast scanning system (Bruker ICON). A silicon tip with a nominal spring constant of 0.4 N/m (ScanAsyst-Air, Bruker) was used for the AFM measurements. The mechanical properties of self-assembled spidroins was measured by a cantilever with a spring constant of ≈34.32 N m^{-1} and a tip radius of 8 nm. Of note, the spring constant of the cantilevers (Bruker, Germany) was calibrated by a sapphire wafer. The morphological and

https://doi.org/10.1021/acsomega.4c02477
ACS Omega 2024, 9, 22441−22449

mechanical data of self-assembled spidroins were processed by the software NanoScope Analysis 1.8.

4.4. Circular Dichroism Analysis. A Jasco J-1500 spectrometer was used to carry out circular dichroism (CD) spectra at 25 °C. The self-assembled spidroins were diluted to 0.1 mg/mL for measurement using glass cuvettes with a path length of 1 cm. Wavelength scans were collected from 185 to 260 nm in 0.5 nm steps with a scan speed of 100 nm/min and a bandwidth of 1.0 nm.

4.5. Fourier-Transform Infrared Spectroscopy. The secondary structure of recombinant spidroins was characterized by Fourier-transform infrared (FTIR) spectroscopy in ATR mode (Bruker OPTIK GmbH Tensor II). For each measurement, the wavenumbers ranged from 400 to 4000 cm^{-1} with 128 scans and a resolution of 8 cm^{-1}. A nitrogen atmosphere was used to avoid interference with the water absorption. In addition, the deconvolution of the amide I band was performed using the PeakFit 4.04 software.

■ ASSOCIATED CONTENT

Supporting Information

The Supporting Information is available free of charge at https://pubs.acs.org/doi/10.1021/acsomega.4c02477.

Rosetta potential energy analysis of wild-type spidroin 2REP and mutant spidroin 2REPM; MaSp1 Rep2, ΔG = −24.6 kcal/mol; MaSp1 Rep2M, ΔG = −25.6 kcal/mol; RMSD and R_g of wild-type spidroin 2REP and mutant spidroin 2REPM; HT curves to clarify the reproducibility of CD signals (PDF)

■ AUTHOR INFORMATION

Corresponding Authors

Cheng Cheng − *School of Pharmaceutical Sciences, Nanjing Tech University, Nanjing 211816, China;* orcid.org/0009-0004-4145-9472; Email: cheng2@njtech.edu.cn

Ke Zheng − *Biomass Molecular Engineering Center and Department of Materials Science and Engineering, School of Forestry and Landscape Architecture, Anhui Agricultural University, Hefei, Anhui 230036, China*; Email: zhengke@ahau.wdu.cn

Authors

Ziyang Chen − *College of Biotechnology and Pharmaceutical Engineering, Nanjing Tech University, Nanjing 211816, China*

Li Liu − *Biomass Molecular Engineering Center and Department of Materials Science and Engineering, School of Forestry and Landscape Architecture, Anhui Agricultural University, Hefei, Anhui 230036, China*

Baoyang Lin − *College of Biotechnology and Pharmaceutical Engineering, Nanjing Tech University, Nanjing 211816, China*

Yongji Xiong − *College of Biotechnology and Pharmaceutical Engineering, Nanjing Tech University, Nanjing 211816, China*

Weiyu Zhu − *School of Pharmaceutical Sciences, Nanjing Tech University, Nanjing 211816, China*

Bingfang He − *School of Pharmaceutical Sciences, Nanjing Tech University, Nanjing 211816, China; College of Biotechnology and Pharmaceutical Engineering, Nanjing Tech University, Nanjing 211816, China;* orcid.org/0000-0002-4502-9531

Complete contact information is available at: https://pubs.acs.org/10.1021/acsomega.4c02477

Notes

The authors declare no competing financial interest.

■ ACKNOWLEDGMENTS

This study was supported by grants from National Key R&D Program of China (2019YFA0905200), the National Natural Science Foundation Youth Fund (22308159), the Natural Science Foundation of Jiangsu Province (BK20220335), the Jiangsu Provincial Association for Science and Technology Youth Talent Support Project (TJ-2023-021), the National Science Foundation of China (22105003), the Anhui Provincial Natural Science Foundation (2008085MB35), and the Jiangsu Students' platform for innovation and entrepreneurship training program (202310291270Y). In addition, we are grateful to the High Performance Computing Center of Nanjing Tech University for supporting the computational resources.

■ REFERENCES

(1) Cheng, C.; Qiu, Y.; Tang, S.; Lin, B.; Guo, M.; Gao, B.; He, B. Artificial Spider Silk Based Programmable Woven Textile for Efficient Wound Management. *Adv. Funct. Mater.* **2022**, *32*, 2107707.

(2) Zhou, Y.; Shen, Q.; Lin, Y.; Xu, S.; Meng, Q. Evaluation of the potential of chimeric spidroins/poly(L-lactic-co-ε-caprolactone) (PLCL) nanofibrous scaffolds for tissue engineering. *Materials Science and Engineering: C* **2020**, *111*, 110752.

(3) Trossmann, V. T.; Scheibel, T. Design of Recombinant Spider Silk Proteins for Cell Type Specific Binding. *Adv. Healthcare Mater.* **2023**, *12*, 2202660.

(4) Qin, N.; Qian, Z.-G.; Zhou, C.; Xia, X.-X.; Tao, T. H. 3D electron-beam writing at sub-15 nm resolution using spider silk as a resist. *Nat. Commun.* **2021**, *12*, 5133.

(5) Vollrath, F.; Knight, D. P. Liquid crystalline spinning of spider silk. *Nature* **2001**, *410*, 541−548.

(6) Bratzel, G.; Buehler, M. J. Sequence-structure correlations in silk: Poly-Ala repeat of N. clavipes MaSp1 is naturally optimized at a critical length scale. *Journal of the Mechanical Behavior of Biomedical Materials* **2012**, *7*, 30−40.

(7) Askarieh, G.; Hedhammar, M.; Nordling, K.; Saenz, A.; Casals, C.; Rising, A.; Johansson, J.; Knight, S. D. Self-assembly of spider silk proteins is controlled by a pH-sensitive relay. *Nature* **2010**, *465*, 236−238.

(8) Hagn, F.; Eisoldt, L.; Hardy, J. G.; Vendrely, C.; Coles, M.; Scheibel, T.; Kessler, H. A conserved spider silk domain acts as a molecular switch that controls fibre assembly. *Nature* **2010**, *465*, 239−242.

(9) Xia, X.-X.; Qian, Z.-G.; Ki, C. S.; Park, Y. H.; Kaplan, D. L.; Lee, S. Y. Native-sized recombinant spider silk protein produced in metabolically engineered Escherichia coli results in a strong fiber. *Proc. Natl. Acad. Sci. U. S. A.* **2010**, *107*, 14059−14063.

(10) Zheng, K.; Ling, S. De Novo Design of Recombinant Spider Silk Proteins for Material Applications. *Biotechnol. J.* **2019**, *14*, 1700753.

(11) Stengel, D.; Saric, M.; Johnson, H. R.; Schiller, T.; Diehl, J.; Chalek, K.; Onofrei, D.; Scheibel, T.; Holland, G. P. Tyrosine's Unique Role in the Hierarchical Assembly of Recombinant Spider Silk Proteins: From Spinning Dope to Fibers. *Biomacromolecules* **2023**, *24*, 1463−1474.

(12) Goldschmidt, L.; Teng, P. K.; Riek, R.; Eisenberg, D. Identifying the amylome, proteins capable of forming amyloid-like fibrils. *Proc. Natl. Acad. Sci. U. S. A.* **2010**, *107*, 3487−3492.

(13) Joel, A.-C.; Rawal, A.; Yao, Y.; Jenner, A.; Ariotti, N.; Weissbach, M.; Adler, L.; Stafstrom, J.; Blamires, S. J. Physico-

chemical properties of functionally adhesive spider silk nanofibres. *Biomater. Sci.* **2023**, *11*, 2139−2150.
(14) Römer, L.; Scheibel, T. The elaborate structure of spider silk. *Prion* **2008**, *2*, 154−161.
(15) Lefèvre, T.; Boudreault, S.; Cloutier, C.; Pézolet, M. Diversity of Molecular Transformations Involved in the Formation of Spider Silks. *J. Mol. Biol.* **2011**, *405*, 238−253.
(16) Han, L.; Zhang, L.; Zhao, T.; Wang, Y.; Nakagaki, M. Analysis of a new type of major ampullate spider silk gene, MaSp1s. *Int. J. Biol. Macromol.* **2013**, *56*, 156−161.
(17) Tokareva, O. S.; Lin, S.; Jacobsen, M. M.; Huang, W.; Rizzo, D.; Li, D.; Simon, M.; Staii, C.; Cebe, P.; Wong, J. Y.; Buehler, M. J.; Kaplan, D. L. Effect of sequence features on assembly of spider silk block copolymers. *J. Struct. Biol.* **2014**, *186*, 412−419.
(18) Thamm, C.; Scheibel, T. Recombinant Production, Characterization, and Fiber Spinning of an Engineered Short Major Ampullate Spidroin (MaSp1s). *Biomacromolecules* **2017**, *18*, 1365−1372.
(19) Li, J.; Zhu, Y.; Yu, H.; Dai, B.; Jun, Y.-S.; Zhang, F. Microbially Synthesized Polymeric Amyloid Fiber Promotes β-Nanocrystal Formation and Displays Gigapascal Tensile Strength. *ACS Nano* **2021**, *15*, 11843−11853.
(20) Arndt, T.; Greco, G.; Schmuck, B.; Bunz, J.; Shilkova, O.; Francis, J.; Pugno, N. M.; Jaudzems, K.; Barth, A.; Johansson, J.; Rising, A. Engineered Spider Silk Proteins for Biomimetic Spinning of Fibers with Toughness Equal to Dragline Silks. *Adv. Funct. Materials* **2022**, *32*, 2200986.
(21) Thompson, M. J.; Sievers, S. A.; Karanicolas, J.; Ivanova, M. I.; Baker, D.; Eisenberg, D. The 3D profile method for identifying fibril-forming segments of proteins. *Proc. Natl. Acad. Sci. U. S. A.* **2006**, *103*, 4074−4078.
(22) Otikovs, M.; Andersson, M.; Jia, Q.; Nordling, K.; Meng, Q.; Andreas, L. B.; Pintacuda, G.; Johansson, J.; Rising, A.; Jaudzems, K. Degree of Biomimicry of Artificial Spider Silk Spinning Assessed by NMR Spectroscopy. *Angewandte Chemie, International Edition.* **2017**, *56*, 12571−12575.
(23) Zeng, R.; Zhang, L.; Luo, Z.; Tang, D. Palindromic Fragment-Mediated Single-Chain Amplification: An Innovative Mode for Photoelectrochemical Bioassay. *Analytical Chemistry* **2019**, *91*, 7835−7841.
(24) Zeng, R.; Luo, Z.; Su, L.; Zhang, L.; Tang, D.; Niessner, R.; Knopp, D. Palindromic Molecular Beacon Based Z-Scheme BiOCl-Au-CdS Photoelectrochemical Biodetection. *Analytical Chemistry* **2019**, *91*, 2447−2454.
(25) Abraham, M. J.; Murtola, T.; Schulz, R.; Páll, S.; Smith, J. C.; Hess, B.; Lindahl, E. GROMACS: High performance molecular simulations through multi-level parallelism from laptops to supercomputers. *SoftwareX* **2015**, *1*, 19−25.
(26) Maier, J. A.; Martinez, C.; Kasavajhala, K.; Wickstrom, L.; Hauser, K. E.; Simmerling, C. ff14SB: Improving the Accuracy of Protein Side Chain and Backbone Parameters from ff99SB. *J. Chem. Theory Comput.* **2015**, *11*, 3696−3713.
(27) Yan, Y.; Zhang, D.; Zhou, P.; Li, B.; Huang, S.-Y. HDOCK: a web server for protein−protein and protein−DNA/RNA docking based on a hybrid strategy. *Nucleic Acids Res.* **2017**, *45*, W365−W373.
(28) Pettersen, E. F.; Goddard, T. D.; Huang, C. C.; Meng, E. C.; Couch, G. S.; Croll, T. I.; Morris, J. H.; Ferrin, T. E. UCSF ChimeraX: Structure visualization for researchers, educators, and developers. *Protein Sci.* **2021**, *30*, 70−82.
(29) Nosé, S.; Klein, M. L. Constant pressure molecular dynamics for molecular systems. *Mol. Phys.* **1983**, *50*, 1055−1076.
(30) Bussi, G.; Donadio, D.; Parrinello, M. Canonical sampling through velocity rescaling. *J. Chem. Phys.* **2007**, *126*, 014101.
(31) Valdés-Tresanco, M. S.; Valdés-Tresanco, M. E.; Valiente, P. A.; Moreno, E. gmx_MMPBSA: A New Tool to Perform End-State Free Energy Calculations with GROMACS. *J. Chem. Theory Comput.* **2021**, *17*, 6281−6291.
(32) Li, J.; Jiang, B.; Chang, X.; Yu, H.; Han, Y.; Zhang, F. Bi-terminal fusion of intrinsically-disordered mussel foot protein fragments boosts mechanical strength for protein fibers. *Nat. Commun.* **2023**, *14*, 2127.
(33) Whittall, D. R.; Baker, K. V.; Breitling, R.; Takano, E. Host Systems for the Production of Recombinant Spider Silk. *Trends Biotechnol.* **2021**, *39*, 560−573.
(34) Li, S.; Zhang, S.; Feng, N.; Zhang, N.; Zhu, Y.; Liu, Y.; Wang, W.; Xin, X. Chiral Inversion and Recovery of Supramolecular Luminescent Copper Nanocluster Hydrogels Triggered by Polyethyleneimine and Polyoxometalates. *ACS Appl. Mater. Interfaces* **2022**, *14*, 52324−52333.
(35) Feng, N.; Wang, Z.; Sun, D.; Zhang, L.; Xin, X.; Sun, P.; Azam, M.; Li, H. Kinetically Controlled Structural Modulation of the Self-Assembled Silver Nanoclusters. *Small* **2024**, *20*, 2305366.
(36) Shen, J.; Xiao, Q.; Sun, P.; Feng, J.; Xin, X.; Yu, Y.; Qi, W. Self-Assembled Chiral Phosphorescent Microflowers from Au Nanoclusters with Dual-Mode pH Sensing and Information Encryption. *ACS Nano* **2021**, *15*, 4947−4955.
(37) Bi, Y.; Wang, Z.; Liu, T.; Sun, D.; Godbert, N.; Li, H.; Hao, J.; Xin, X. Supramolecular Chirality from Hierarchical Self-Assembly of Atomically Precise Silver Nanoclusters Induced by Secondary Metal Coordination. *ACS Nano* **2021**, *15*, 15910−15919.
(38) Feng, N.; Wang, Z.; Sun, D.; Sun, P.; Xin, X.; Cheng, X.; Li, H. Circularly Polarized Phosphorescence from Cocrystallization of Atomic Precise Silver Nanoclusters with Tartaric Acid. *Adv. Opt. Mater.* **2022**, *10*, 2102319.

https://doi.org/10.1021/acsomega.4c02477
ACS Omega 2024, 9, 22441−22449